

Wearable, Breathable and Waterproof Triboelectric Nanogenerators for Harvesting Human Motion and Raindrop Energy

Wei Yuan, Chuguo Zhang, Baofeng Zhang, Xuelian Wei, Ou Yang, Yuebo Liu, Lixia He, Shengnan Cui, Jie Wang,* and Zhong Lin Wang

Smart textiles capable of harvesting biomechanical energy via triboelectric effect have been well developed in the field of self-powered wearable electronic products. However, it is still a challenge to manufacture self-charging wearable electronic products with features of high triboelectric output, breathability and water resistance, simultaneously. Herein, a multifunctional wearable triboelectric nanogenerator (MW-TENG) is designed with the functions of flexibility, excellent water resistance and air permeability to provide comfort and convenience in practical application. The maximum peak power density of the MW-TENG can reach 1.03 W m^{-2} under the frequency of 3 Hz. Moreover, the MW-TENG can be embedded in clothes and shoes to drive wearable electronic devices by harvesting human mechanical energy and raindrop energy. This work not only presents a kind of MW-TENG with the functions of flexible, breathable, and waterproof, but also provides a practical strategy to design multifunctional self-powered wearable electronic devices.

1. Introduction

The rapid development in wearable technologies and growing production of wearable electronic devices, which bring much

W. Yuan, C. Zhang, B. Zhang, X. Wei, O. Yang, Y. Liu, L. He, S. Cui, J. Wang, Z. L. Wang
 Beijing Institute of Nanoenergy and Nanosystems
 Chinese Academy of Sciences
 Beijing 100083, China
 E-mail: wangjie@binn.cas.cn

W. Yuan, C. Zhang, B. Zhang, X. Wei, O. Yang, L. He, S. Cui, J. Wang, Z. L. Wang
 School of Nanoscience and Technology
 University of Chinese Academy of Sciences
 Beijing 100049, P. R. China

Y. Liu, J. Wang
 Center on Nanoenergy Research
 School of Physical Science and Technology
 Guangxi University
 Nanning 530004, P. R. China

Z. L. Wang
 School of Materials Science and Engineering
 Georgia Institute of Technology
 Atlanta, GA 30332, USA

 The ORCID identification number(s) for the author(s) of this article can be found under <https://doi.org/10.1002/admt.202101139>.

DOI: [10.1002/admt.202101139](https://doi.org/10.1002/admt.202101139)

convenience in our lives, have received extensive attention.^[1–3] However, a key issue obstructing the way to the extensive commercial applications is their limited power sources.^[4–6] The traditional batteries cannot provide a continuous power supply resulting from frequent charging times and battery replacements.^[7–9] To address this issue, many strategies including photovoltaic solar cells, wind power generation are employed. Nevertheless, their performance is significantly affected by weather and external factors, making it impossible to achieve continuous energy output.^[10–13] On the other hand, mechanical motions such as the movement of the human body can produce a variety of low-frequency mechanical energy in daily activities.^[14,15] However, most of these energies are ignored. Thus, breaking

through technical limitations to develop a device that can efficiently collect various mechanical energy to drive wearable electronic devices is necessary and urgent.^[16]

Based on the coupling effect of triboelectrification and electrostatic induction, triboelectric nanogenerators (TENG) is developed to convert ubiquitous low-frequency and tiny mechanical energy into electricity.^[17–21,30–34] TENG is widely used in self-powered systems, active sensors, high voltage power supply and sustainable blue energy due to its advantages of light weight, small size, high efficiency, and wide selection of materials.^[23,26] Recently, more and more researches have been devoted to obtaining energy from body movement and the external environment by using TENG technology in a convenient and effective way.^[24,25] In previous studies, self-powered wearable TENGs were designed, however, an uncomfortable feeling is fed back due to the poor breathability of the ethylene-vinyl acetate (EVA) film selected.^[22] More recently, self-powered textile was created to enhance the air permeability by hybrid nanogenerators and solar cells for wearable electronics.^[27] Apart from the energy harvesting from random body movement, it also achieves the purpose of collecting outdoor sunshine simultaneously. However, solar energy is affected by the fluctuating intermittent nature of solar irradiation, such as rainy days, causing a major hurdle for the continuous utilization of solar energy. Thus, as a complementary part, designing a new wearable device that harvests the distributed mechanical energy of the human body

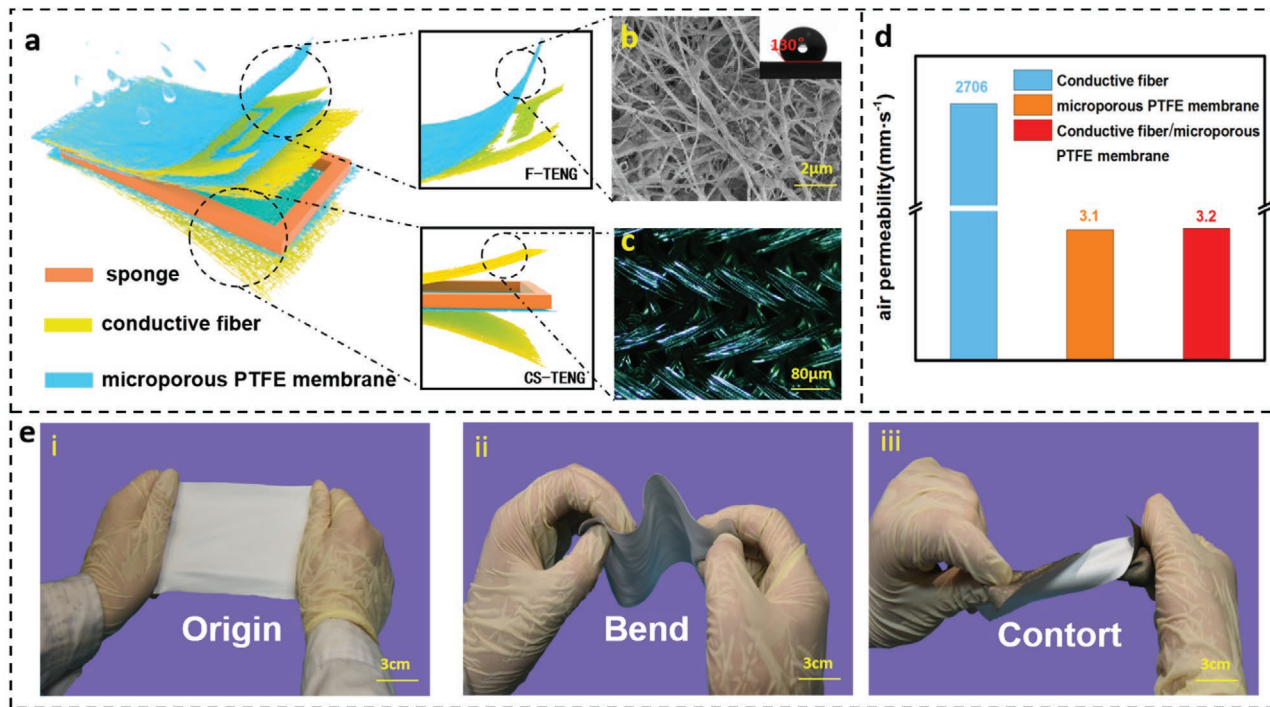


Figure 1. Device structure and performance demonstration of MW-TENG. a) Schematic illustration of the three-dimensional network structure of MW-TENG. b) SEM image and water contact angle image of microporous PTFE membrane. c) The image of the conductive fiber is magnified 135 times using an optical microscope. d) The air permeability of microporous PTFE membrane, conductive fiber and microporous PTFE membrane/conductive fiber. e) Photographs of the flexible MW-TENG in (i) origin, (ii) bend and (iii) contorting conditions.

while harvesting raindrop energy on a rainy day would greatly promote the development of wearable electronic devices. To achieve this goal, the materials selected have to be waterproof to ensure that TENG has the ability to harvest raindrop energy when raining. Besides, it also protects TENG from the impact of environmental humidity when harvesting mechanical energy, because the output of the TENG greatly reduces in a high humidity environment.^[27–30] Meanwhile, air breathability is highly required to provide a comfortable contact. Therefore, the challenge of simultaneously maintaining both good air permeability and water resistance needs to be addressed.

Herein, we rationally designed a flexible multifunctional wearable triboelectric nanogenerator (MW-TENG), which is composed of a contact-separation mode triboelectric nanogenerator (CS-TENG) and a free-standing triboelectric-layer triboelectric nanogenerator (F-TENG). The CS-TENG and the F-TENG all consist of microporous polytetrafluoroethylene (PTFE) membrane as the triboelectric materials and the conductive fiber as the conductive materials. The microporous PTFE membrane film outside ensures a good air permeability and waterproof function because of its porosity and hydrophobicity. While the conductive fiber further improves a comfort feeling by the air permeability and flexibility. Taking the advantages, CS-TENG harvests the mechanical energy of the human body and F-TENG harvests raindrop energy. As a result, through the above-mentioned structural design, MW-TENG enables to simultaneously harvest both raindrop energy and human movement energy. The maximum peak power density of the MW-TENG has been reached at 1.03 W m^{-2} under the tapping frequency of 3 Hz. This

work not only presents a kind of MW-TENG with the functions of flexible, breathable and waterproof, but also provides a self-powered strategy to drive wearable electronics.

2. Result and Discussion

As shown in Figure 1a, multifunctional wearable triboelectric nanogenerator (MW-TENG) is composed of a contact-separation triboelectric nanogenerator (CS-TENG) and free-standing triboelectric-layer triboelectric nanogenerator (F-TENG). The CS-TENG, which can be used to harvest human mechanical energy, is fabricated in the inner layer by two conductive fiber layers and a microporous PTFE membrane. In addition, a hollow sponge is utilized to ensure the efficient separation of CS-TENG. The F-TENG consisting of an interdigital electrode structure in the internal and a microporous PTFE membrane on the upper surface, is installed on the surface of the CS-TENG to harvest raindrop energy on rainy days. In the two types of TENGs, the conductive fiber is used as electrodes of TENG and the microporous PTFE membrane is applied as triboelectric materials. Meanwhile, a microporous PTFE membrane is sandwiched between CS-TENG and F-TENG to guarantee the free operation of two types of TENGs without the interaction effect. Figure 1b shows the hole surface morphologies of the microporous PTFE membrane observed by scanning electron microscopy (SEM), which fully verifies the good air permeability of MW-TENG. The water contact angle of 130° for the microporous PTFE membrane inserted on the top

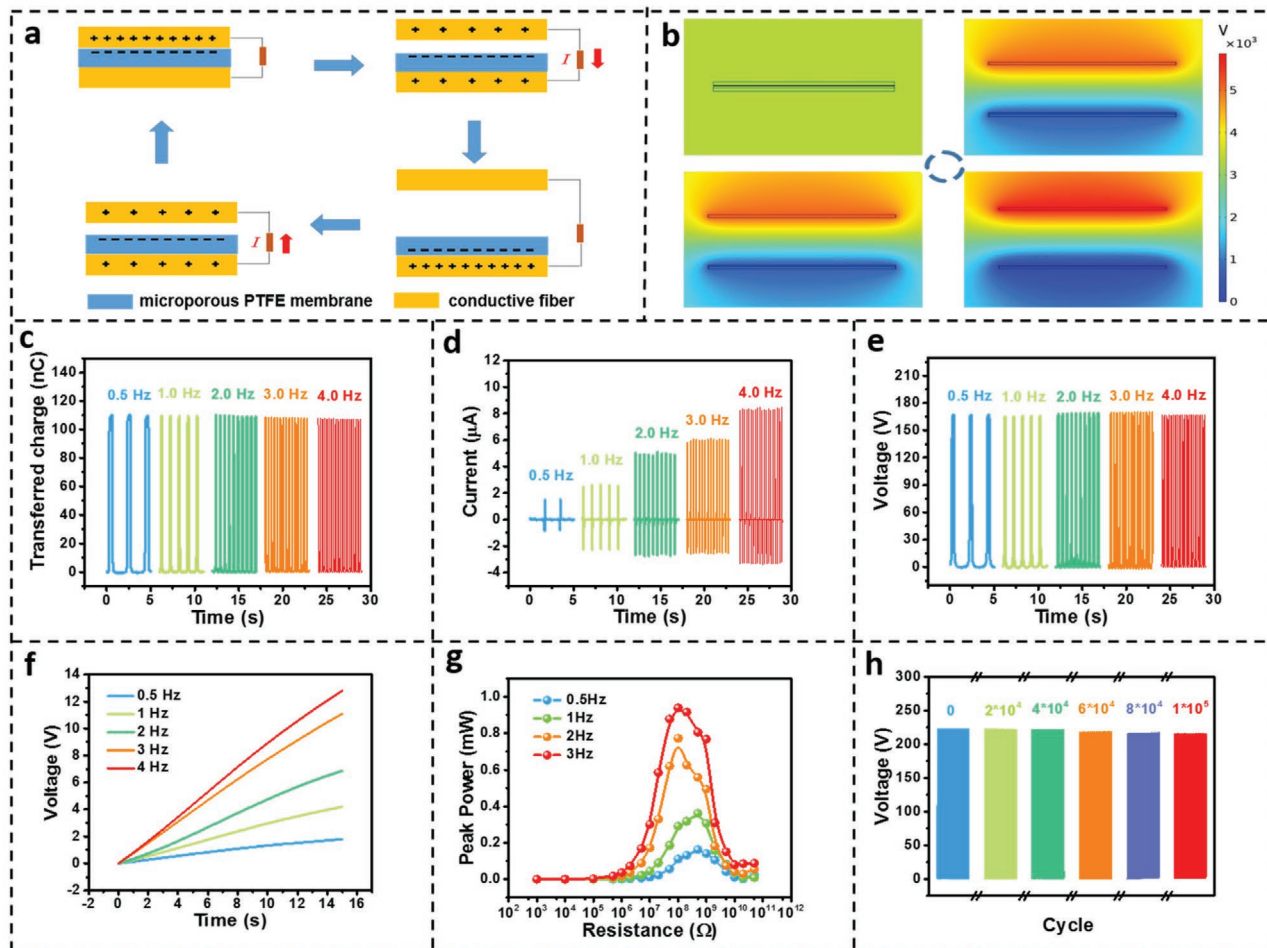


Figure 2. Working mechanism and electrical output performance of the CS-TENGs. a) Schematic diagrams showing the working principle of the CS-TENGs. b) Numerical calculation of the corresponding electrical potential distribution by the COMSOL software. c) Q_{SC} and e) V_{OC} of the CS-TENGs under different frequencies (0.5 – 4 Hz). f) Charging curves at different frequencies when CS-TENGs charged 0.47 μ F capacitors. g) The variation of peak power of the CS-TENGs under different frequencies (0.5 – 4 Hz) with different external load resistances. h) Stability test of the CS-TENGs under continuous impact for 10⁶ times. Data is collected every 20 000 cycles.

right reflects that the hydrophobic microporous PTFE membrane can effectively prevent water and rain drop to achieve the function of waterproof. The image of the conductive fiber in Figure 1c clearly shows that the silver fiber is woven into the fabric to form a conductive network, indicative of its conductivity of 40 000 S m⁻¹. Moreover, the holes in conductive fibers provide a good air permeability. To better demonstrate the air permeability of MW-TENG, which is an important index to judge the comfort of fabric, the air permeability is measured as illustrated in Figure 1d. It is easy to find that the MW-TENG has good breathability and the air permeability of MW-TENG is dominated by the microporous PTFE membrane. Meanwhile, excellent flexibility is another crucial demand for clothing as well. As presented in Figure 1e, the MW-TENGs can realize all kinds of deformation, such as bent and contorted, to adapt the various deformation of human motion. All these functions of MW-TENG fully indicate that it is a promising candidate for the design and manufacture of human clothing.

In order to research the output performance of the CS-TENG part, a linear motor is used to test the output performance of CS-

TENG with the size of 3 × 3 cm. The working mechanism of CS-TENG is shown in Figure 2a, which can be attributed to the coupling effect of contact electrification and electrostatic induction. In the initial stage, the microporous PTFE membrane contacts with the upper conductive fiber. Since the frictional electrical polarity of the conductive fiber and the microporous PTFE membrane are opposite, the microporous PTFE membrane and the conductive fiber will exhibit negative and positive charges, respectively. When the two surfaces move away from each other, the electric potential of the conductive fiber layer rises and prompts the electrons of the lower conductive fiber to flow to the upper conductive fiber electrode through the external circuit. As the gap between the two frictionally charged surfaces continues to increase to complete separation, all electrons will flow to the upper conductive fiber electrode. When the conductive fiber approaches the microporous PTFE membrane again, the relevant flowing electrons transfer from the upper conductive fiber to the lower conductive fiber electrode through the external circuit. Thus, an alternating current is generated. In addition, to understand the above mechanism of the power generation process, COMSOL

software is utilized to simulate the relative potential of the conductive fiber and the microporous PTFE membrane under the different states (Figure 2b). The transferred charges (Q_{SC}), short circuit current (I_{SC}) and open circuit voltage (V_{OC}) are measured at frequencies from 0.5 to 4 Hz, respectively. With the increase of frequency, Q_{SC} and V_{OC} remain basically unchanged (110 nC and 168 V, respectively), the maximum charge density can reach 122 $\mu\text{C m}^{-2}$. Meanwhile, the I_{SC} increase with frequency from 1.5 μA at 0.5 Hz to 8.3 μA at 4 Hz (Figure 2c–e) and the corresponding reason is that the changing rate of I_{SC} increases with the frequency. The explanation of the relevance of the frequency and short circuit current can be obtained in Note S1 in the supporting information. This result indicates that a higher frequency of human motion is beneficial for the output performance of CS-TENG. Figure 2f displays the capacitor charging characteristics of CS-TENG at different frequencies. By using the circuit diagram of Figure S1 (supporting information), it takes CS-TENG 15 s to charge the 0.47 μF capacitor to 1.80, 4.21, 6.86, 11.11, and 12.80 V at the various operative frequencies of 0.5, 1, 2, 3, and 4 Hz, respectively. Figure 2g depicts the peak power measured by externally connecting different resistance loads from 1 $\text{k}\Omega$ to 50 $\text{G}\Omega$ under

the different impact frequencies (0.5–3 Hz). The maximum peak power improves from 0.16 mW at 0.5 Hz to 0.93 mW at 3 Hz and the maximum peak power density of the CS-TENG can reach 1.03 W m^{-2} under the tapping frequency of 3 Hz. Meanwhile, the currents of CS-TENG with different resistances are measured under the frequency from 0.5 to 3 Hz, respectively (Figure S2, Supporting Information) and the current of CS-TENG decreases with the resistance increase. The durability test of wearable electronic devices suggests that the V_{OC} , Q_{SC} and I_{SC} maintain 96.9% (223 V to 216 V), 96.8% (93 to 90 nC) and 95% (22 to 20.9 μA) after 100 000 cycles of impacts (the data is harvested every 20 000 times) (Figure 2h and Figure S3 in supporting information), reflecting CS-TENG of a high stability. Figure S4, Supporting Information, shows the corresponding SEM images of the microporous PTFE membrane interval 20 000 cycles test. It is obvious to found that the surface of the microporous PTFE membrane almost keeps unchanged during this process, which demonstrates the robustness of the CS-TENG.

Figure 3a shows a working mechanism of the F-TENG part fabricated by a microporous PTFE membrane and interdigital conductive fiber for the harvesting of rainwater energy. The

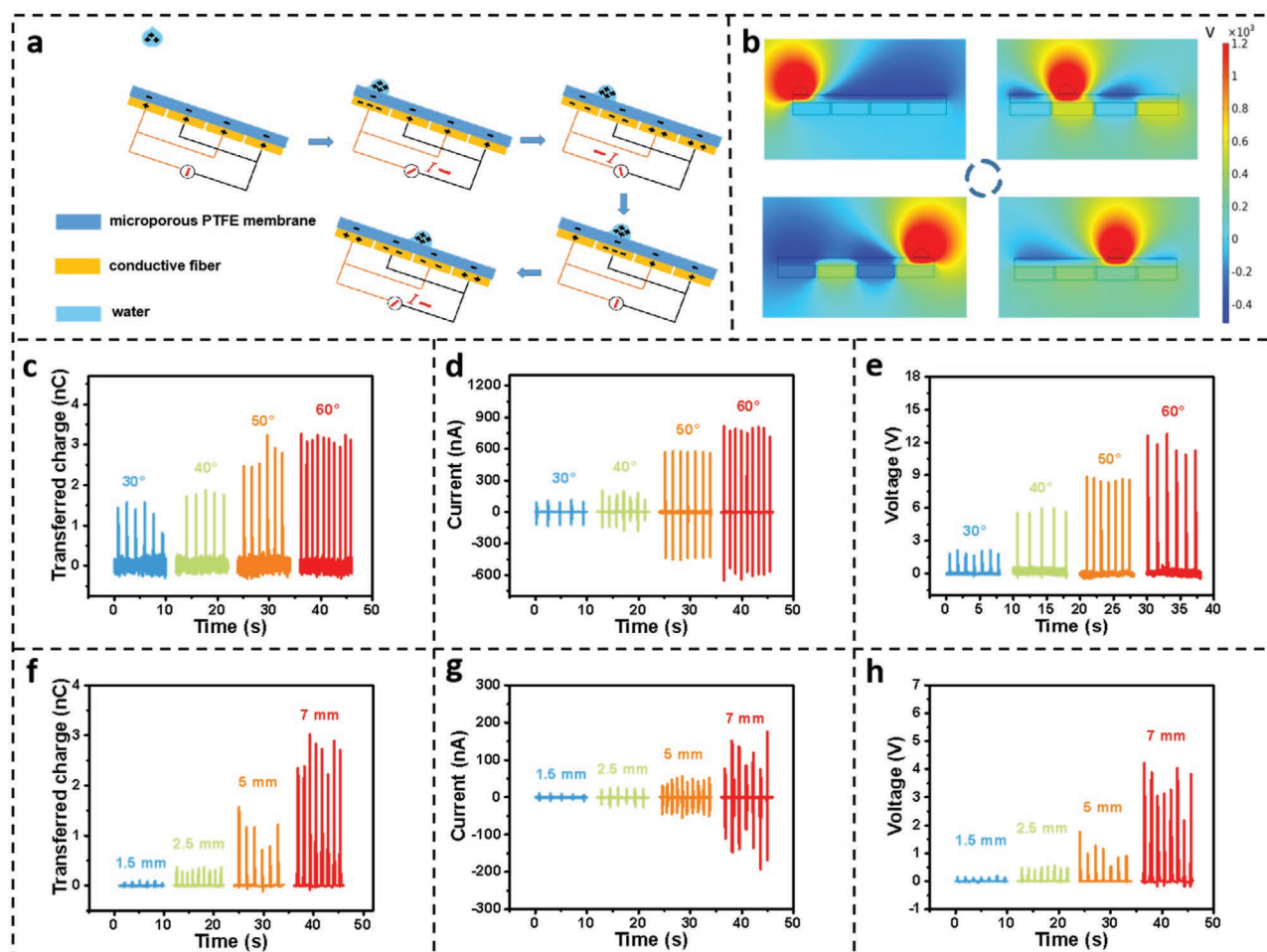


Figure 3. Working mechanism and electrical output performance of the TENGs. a) Schematic diagrams showing the working principle of the TENGs. b) Numerical calculation of the corresponding electrical potential distribution by the COMSOL software. c) Q_{SC} , d) I_{SC} and e) V_{OC} of the TENGs under different angles between the straight line of raindrops and the surface of TENG (30°–60°). f) Q_{SC} , g) I_{SC} and h) V_{OC} of the TENGs under different diameters of raindrops.

operation mode of F-TENG is based on the independent friction layer mode and the interdigital electrodes with the multiple units are divided into two kinds of electrode to improve output performance of the short-circuit current of F-TENG. As reported, the water droplets in the air will obtain a corresponding positive charge due to the friction with the air.^[30] Thus, when raindrops contact the microporous PTFE membrane, the positive charge in the raindrop will further increase to generate the higher potential of the microporous PTFE membrane. At this time, the lower interdigital electrode unit will show electronegativity and generate the related current in the external circuit. When the raindrops begin to slide toward the other interdigital electrode, the negative charge of the original interdigital electrode decreases, and the positive charge of the other interdigital electrode increases, thereby generating a current in the other direction. As the raindrops completely slide to the other interdigital electrode, the lower interdigital electrode induces negative charges, and the other interdigital electrodes induce positive charges. In addition, the COMSOL software is used to simulate the electric potential between the conductive fiber and the microporous PTFE membrane to understand the proposed power generation process mechanism (Figure 3b). Figure S5 in supporting information shows a photograph of the interdigital electrode structure of F-TENG. Figure 3c–e shows the various output performances of the F-TENG at the different incident angles of raindrops ($30^\circ - 60^\circ$). The Q_{SC} of the F-TENG increased from 1.35 to 3.18 nC, the I_{SC} increased from 103.72 to 781.81 nA and the V_{OC} of the F-TENG increased from 1.98 V to 11.80 V as the incident angle of raindrops increased. It suggests that the larger the incident angle of the raindrop, the higher the output of the F-TENG. Moreover, the output performance of the F-TENG with the different diameters of raindrops are measured in detail (Figure 3f–h). We control the size of the raindrop diameter by attaching different sized pipette tips to the bottom of the burette. The Q_{SC} of the F-TENG increased from 0.09 to 2.65 nC, the I_{SC} increased from 9.62 to 117.89 nA and the V_{OC} of the F-TENG increased from 0.157 to 3.46 V with the increase of raindrop diameter. The corresponding reason is that the contact area of raindrops to F-TENG increases with the increase of raindrop diameter.

As discussed above, the MW-TENG not only can harvest the energy of mechanical energy when the human body moves by the CS-TENG part, but can also be easily deployed to harvest raindrop energy from the rainfall environment by the F-TENG part. Figure 4a shows the MW-TENG with the size of 10×10 cm harvesting mechanical energy from different parts of the human body, the arm, the leg, and the foot. The electric energy harvested from body sports can be stored in different stored energy devices. The MW-TENG which is attached to the elbow and knee, mainly collects the mechanical energy of the elbow and knee joint flexion. The MW-TENG which is attached to the bottom of the foot, mainly collects the mechanical energy of the foot stepping and lifting while walking. Figure 4b shows the charging curve when MW-TENGs charge $0.47\mu\text{F}$ capacitors in different parts of the human body. When MW-TENG is placed on the arms, legs and feet to harvest the mechanical energy of the human body, the $0.47\mu\text{F}$ capacitor is charged to 2.24, 4.49, and 5.93 V within 5 s. The capacitors of 1 and $2.2\mu\text{F}$ are also charged by MW-TENG (Figure S6 in supporting information).

It takes 8 s to charge the voltage of capacitors of 0.47, 1, and $2.2\mu\text{F}$ to 1.24, 2.09, 3.48 V through MW-TENG on the arms, 5 s to 1.48, 3.16, 4.49 V through MW-TENG on the leg and 7 s to 2.00, 3.52, 7.68 V through MW-TENG on the arms. In order to prove their applicability, MW-TENG is designed to embed in traffic safety suit. When wearing clothes fabricated by MW-TENG, LED warning signs on the vest can be lighted up during walking or tapping the MW-TENG (Figure 4c and Supporting Information Video S1). On the other hand, the watch is operated when MW-TENG harvests mechanical energy (Figure S9 and Video S3, Supporting Information). Moreover, the shoulder lights installed on the clothes are lit by raindrop energy (Figure 4d and Supporting Information Video S2). The raindrops falling on MW-TENG can be clearly seen in the upper right of Figure 4d. When the MW-TENG is fabricated in three body parts, the corresponding Q_{SC} , I_{SC} and V_{OC} are measured, respectively (Figure 4e–g). The highest output performance is $0.3\mu\text{C}$, $4\mu\text{A}$, and 125 V; $0.12\mu\text{C}$, $0.8\mu\text{A}$, 32 V and $0.15\mu\text{C}$, $2\mu\text{A}$, 87 V, respectively, when the MW-TENG is attached to the sole of the foot, arm and leg. Figure S7 (support information) shows the measured peak power and corresponding current when MW-TENG is attached to different parts of the body and connected to different loads at $1\text{ k}\Omega \approx 100\text{ G}\Omega$. It indicates that the MW-TENG which is attached to the arms and legs can obtain a maximum peak power of 0.17 mW and 0.35 mW respectively, under a load of $20\text{ M}\Omega$. The maximum peak power of 1.35 mW can be obtained at a $50\text{ M}\Omega$ load when TENG is attached to the sole of the foot. At the same time, the output current is almost stable when the load resistance is lower than $20\text{ M}\Omega$ while it significantly reduces as the load resistance changes from $20\text{ M}\Omega$ to $5\text{ G}\Omega$. What is more, MW-TENG can exhibit stable output performance in rain. Figure 4h and Figure S8 (supporting information) prove that the output performance of the CS-TENG part hardly changes in the rainfall environment compared with that before rain owing to the protection of water-proof design. On the other hand, rainwater collected in the natural environment and showerheads are used to simulate actual rainfall conditions. Figure 4i–j shows the output performance of F-TENG in harvesting raindrop energy in a realistic rainfall environment. The maximum short circuit current and maximum open circuit voltage are $0.25\mu\text{A}$ and 66 V. As a result, by the rational combination of CS-TENG and F-TENG, the as-prepared MW-TENG provides a practical strategy with wearable, breathable and waterproof properties for self-powered wearable electronic devices.

3. Conclusion

In summary, we design a MW-TENG composed of a contact-separation triboelectric nanogenerator (CS-TENG) and a free-standing triboelectric-layer triboelectric nanogenerator (F-TENG) with a microporous PTFE membrane as the triboelectric materials and the conductive fiber as the conductive material to provide breathable and waterproof performance. The MW-TENG not only can harvest the energy of mechanical energy when the human body moves by CS-TENG part, but can also be easily deployed to harvest raindrop energy from the rainfall environment by the F-TENG part. Thus,

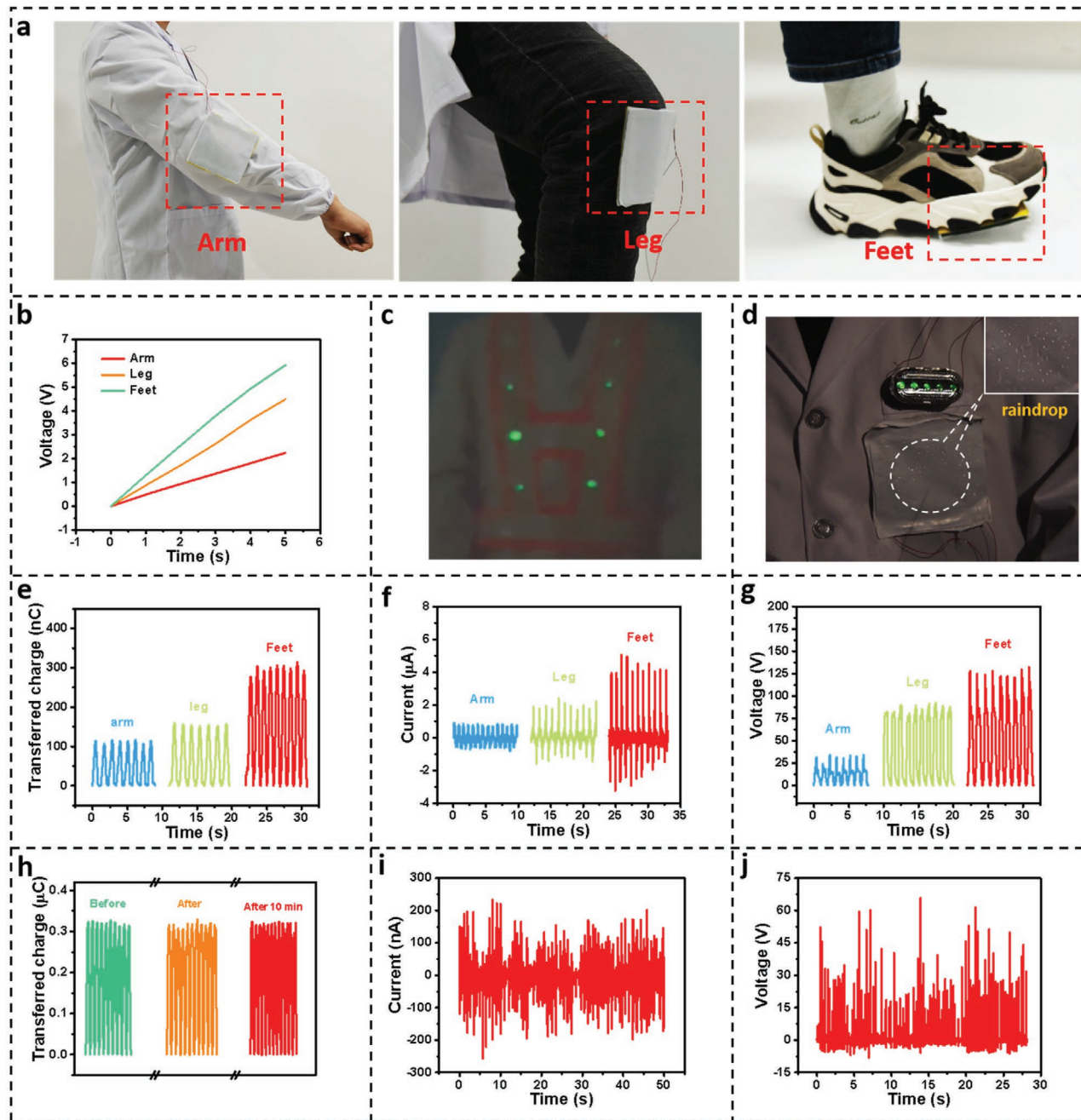


Figure 4. The output performance and application of MW-TENG in human movement mechanical energy collection and raindrop energy collection. a) Schematic diagram of MW-TENG attached to different parts of the body. b) Charging curves at different body parts when MW-TENG charged 0.47 μF capacitors. Demonstration of lighting up the LEDs by c) human movement and d) rainfall, on the upper right is an image of raindrops falling on MW-TENG. e) Q_{SC} , f) I_{SC} and g) V_{OC} of MW-TENG is attached to the different parts of the body. The stability test of CS-TENG and F-TENG in rainfall, h) V_{OC} of CS-TENG before and after rainfall. i) I_{SC} and j) V_{OC} of F-TENG collecting raindrop energy.

the maximum peak power density of MW-TENG can reach 1.03 W m^{-2} . Moreover, the MW-TENG can be embedded in clothes and shoes to power the relevant electronic devices by harvesting human mechanical energy and raindrop energy. This work not only presents a kind of MW-TENG with the functions of flexible, breathable, and waterproof, but also provide a self-powered strategy to drive wearable electronics.

4. Experimental Section

Materials: A microporous PTFE membrane is used for the triboelectric materials, and conductive fiber is used for the conductive layer. The microporous PTFE membrane was injected with negative ions using an air-ionization gun.

Fabrication of the CS-TENG: First, a laser cutter (PLS6.75, Universal Laser Systems) was used to cut acrylic sheets (6 cm \times 6 cm \times 3 mm). Then the foam (6 cm \times 6 cm \times 1 mm) was attached to the acrylic sheet

($6\text{ cm} \times 6\text{ cm} \times 3\text{ mm}$) to achieve effective contact-separation of CS-TENG. Finally, the conductive fiber ($3\text{ cm} \times 3\text{ cm}$) and the microporous PTFE membrane ($6\text{ cm} \times 6\text{ cm} \times 60\text{ }\mu\text{m}$) were attached to the foam. On the other hand, the conductive fiber ($3\text{ cm} \times 3\text{ cm}$) was attached to the acrylic sheet ($6\text{ cm} \times 6\text{ cm} \times 3\text{ mm}$) as the other conductive layer.

Fabrication of the F-TENG: First, a laser cutter (PLS6.75, Universal Laser Systems) was used to cut acrylic sheets ($15\text{ cm} \times 12\text{ cm} \times 3\text{ mm}$). Then, the conductive fiber ($12\text{ cm} \times 10\text{ cm}$) which was cut into interdigital electrodes with 3mm pitch was attached to the acrylic sheet ($15\text{ cm} \times 12\text{ cm} \times 3\text{ mm}$). Finally, the microporous PTFE membranes ($15\text{ cm} \times 12\text{ cm} \times 60\text{ }\mu\text{m}$) were attached to the conductive fiber ($12\text{ cm} \times 10\text{ cm}$). When we measured, we tilted F-TENG to a certain angle to facilitate raindrops to slide off the PTFE surface.

Fabrication of the MW-TENG: First, two sets of a conductive fiber ($10\text{ cm} \times 10\text{ cm}$) are attached to a microporous PTFE membrane($10\text{ cm} \times 10\text{ cm} \times 60\text{ }\mu\text{m}$). Then, a hollow square frame of foam ($10\text{ cm} \times 10\text{ cm} \times 2\text{ mm}$) was attached to one set of the microporous PTFE membrane ($10\text{ cm} \times 10\text{ cm} \times 60\text{ }\mu\text{m}$) and the other set of the conductive fiber ($10\text{ cm} \times 10\text{ cm}$) to compose the CS-TENG part. After that, a laser cutter (PLS6.75, Universal Laser Systems) was used to cut the conductive fiber ($10\text{ cm} \times 10\text{ cm}$) into interdigital electrodes with a 3 mm gap and then it was attached to the microporous PTFE membrane ($10\text{ cm} \times 10\text{ cm} \times 60\text{ }\mu\text{m}$) to achieve the fabrication of the F-TENG. Finally, the F-TENG and the CS-TENG are integrated.

Electrical Measurement of the TENGs: For the electric output measurement of the MW-TENG, CS-TENG and F-TENG, the programmable electrometer (Keithley model 6514) was utilized to measure the transferred charges and short-circuit current. The mixed domain oscilloscope (MDO3024) was utilized to test the open-circuit voltage. A potentiostat (Biologic, VMP3) was utilized to test the voltage of the capacitor in the charging capacitor test. The vertical contact separation motion was carried out by a linear motor (TSMV120-1S).

COMSOL Simulation: The 2D potential distribution between the microgaps of the triboelectric interface was calculated using the commercial software COMSOL. Copper foil, which was used to replace conductive fibers with a thickness of $200\text{ }\mu\text{m}$ were used as electrode and triboelectric film. The PTFE with a thickness of $60\text{ }\mu\text{m}$ film were used as a triboelectric film. The gap distance ranges from 0 to 5 mm. The surface charge density of the PTFE film was set at $50\text{ }\mu\text{C m}^{-2}$.

Air Permeability Test: The air permeability was measured by using an air permeability apparatus (YG461E, Qingdao Standard Testing Co., Ltd., China) according to the ISO 9237:1995 standard test method under 100 pa pressure drop.

Supporting Information

Supporting Information is available from the Wiley Online Library or from the author.

Acknowledgements

W.Y., C.Z., and B.Z. contributed equally to this work. The research was supported by the National Key R & D Project from Minister of Science and Technology (2016YFA0202701), National Natural Science Foundation of China (Grant Nos. 61774016, 21773009, 51432005, 5151101243, and 51561145021), China Postdoctoral Science Foundation (2019M660587) and Beijing Municipal Science & Technology Commission (Z17110000317001, Z171100002017017, Y3993113DF), the Fundamental Research Funds for the Central Universities (E1E46802). The authors also thank Likang Sun for this work.

Conflict of Interest

The authors declare no conflict of interest.

Data Availability Statement

Research data are not shared.

Keywords

triboelectric nanogenerators, mechanical energy harvesting, raindrop energy, waterproof, wearable electronics

Received: September 1, 2021

Revised: October 15, 2021

Published online:

- [1] H. Guo, M. H. Yeh, Y. Zi, Z. Wen, J. Chen, G. Liu, C. Hu, Z. L. Wang, *ACS Nano* **2017**, *11*, 4475.
- [2] J. Luo, W. Gao, Z. L. Wang, *Adv. Mater.* **2021**, *33*, 2004178.
- [3] S. Li, J. Wang, W. Peng, L. Lin, Y. Zi, S. Wang, G. Zhang, Z. L. Wang, *Adv. Energy Mater.* **2017**, *7*, 1602832.
- [4] M. T. Rahman, S. M. S. Rana, M. Salauddin, P. Maharjan, T. Bhatta, J. Y. Park, *Adv. Energy Mater.* **2020**, *10*, 1903663.
- [5] C. Wu, P. Jiang, W. Li, H. Guo, J. Wang, J. Chen, M. R. Prausnitz, Z. L. Wang, *Adv. Funct. Mater.* **2019**, *30*, 1907378.
- [6] J. Wang, S. Li, F. Yi, Y. Zi, J. Lin, X. Wang, Y. Xu, Z. L. Wang, *Nat. Commun.* **2016**, *7*, 12744.
- [7] W. Gao, S. Emaminejad, H. Y. Y. Nyein, S. Challa, K. Chen, A. Peck, H. M. Fahad, H. Ota, H. Shiraki, D. Kiriya, D. H. Lien, G. A. Brooks, R. W. Davis, A. Javey, *Nature* **2016**, *529*, 509.
- [8] X. J. Pu, H. Y. Guo, J. Chen, X. Wang, Y. Xi, C. G. Hu, Z. L. Wang, *Sci. Adv.* **2017**, *3*, e1700694.
- [9] H. Y. Guo, X. J. Pu, J. Chen, Y. Meng, M. H. Yeh, G. L. Liu, Q. Tang, B. D. Chen, D. Liu, S. Qi, C. S. Wu, C. G. Hu, J. Wang, Z. L. Wang, *Sci. Rob.* **2018**, *3*, eaat2516.
- [10] Z. L. Wang, *Adv. Energy Mater.* **2020**, *10*, 2000137.
- [11] L. Zhou, D. Liu, J. Wang, Z. L. Wang, *Friction* **2020**, *8*, 481.
- [12] Z. L. Wang, A. C. Wang, *Mater. Today* **2019**, *30*, 34.
- [13] Y. Zi, J. Wang, S. Wang, S. Li, Z. Wen, H. Guo, Z. L. Wang, *Nat. Commun.* **2016**, *7*, 10987.
- [14] Z. Zhao, Y. Dai, D. Liu, L. Zhou, S. Li, Z. L. Wang, J. Wang, *Nat. Commun.* **2020**, *11*, 6186.
- [15] J. Chen, H. Guo, X. He, G. Liu, Y. Xi, H. Shi, C. Hu, *ACS Appl. Mater. Interfaces* **2016**, *8*, 736.
- [16] C. Zhang, L. He, L. Zhou, O. Yang, W. Yuan, X. Wei, Y. Liu, L. Lu, J. Wang, Z. L. Wang, *Joule* **2021**, *5*, 1613.
- [17] W. Liu, Z. Wang, G. Wang, G. Liu, J. Chen, X. Pu, Y. Xi, X. Wang, H. Guo, C. Hu, Z. L. Wang, *Nat. Commun.* **2019**, *10*, 1426.
- [18] J. Wang, C. Wu, Y. Dai, Z. Zhao, A. Wang, T. Zhang, Z. L. Wang, *Nat. Commun.* **2017**, *8*, 88.
- [19] R. Cheng, K. Dong, L. Liu, C. Ning, P. Chen, X. Peng, D. Liu, Z. L. Wang, *ACS Nano* **2020**, *14*, 15853.
- [20] K. Dong, X. Peng, Z. L. Wang, *Adv. Mater.* **2020**, *32*, 1902549.
- [21] J. Wang, X. Li, Y. Zi, S. Wang, Z. Li, L. Zheng, F. Yi, S. Li, Z. L. Wang, *Adv. Mater.* **2015**, *27*, 4830.
- [22] Y. C. Lai, Y. C. Hsiao, H. M. Wu, Z. L. Wang, *Adv. Sci.* **2019**, *6*, 1801883.
- [23] K. Dong, X. Peng, J. An, A. C. Wang, J. Luo, B. Sun, J. Wang, Z. L. Wang, *Nat. Commun.* **2020**, *11*, 2868.
- [24] J. Xiong, P. Cui, X. Chen, J. Wang, K. Parida, M. F. Lin, P. S. Lee, *Nat. Commun.* **2018**, *9*, 4280.
- [25] J. Chen, Y. Huang, N. Zhang, H. Zou, R. Liu, C. Tao, X. Fan, Z. L. Wang, *Nat. Energy* **2016**, *1*, 16138.
- [26] X. Peng, K. Dong, C. Y. Ye, Y. Jiang, S. Y. Zhai, R. W. Cheng, D. Liu, X. P. Gao, J. Wang, Z. L. Wang, *Sci. Adv.* **2020**, *6*, eaba9624.

- [27] Z. Wen, M. H. Yeh, H. Y. Guo, J. Wang, Y. L. Zi, W. D. Xu, J. N. Deng, L. Zhu, X. Wang, C. G. Hu, L. P. Zhu, X. H. Sun, Z. L. Wang, *Sci. Adv.* **2016**, *2*, e1600097.
- [28] W. Xu, H. Zheng, Y. Liu, X. Zhou, C. Zhang, Y. Song, X. Deng, M. Leung, Z. Yang, R. X. Xu, Z. L. Wang, X. C. Zeng, Z. Wang, *Nature* **2020**, *578*, 392.
- [29] B. Kil Yun, H. Soo Kim, Y. Joon Ko, G. Murillo, J. Hoon Jung, *Nano Energy* **2017**, *36*, 233.
- [30] X. Liu, A. Yu, A. Qin, J. Zhai, *Adv. Mater. Technol.* **2019**, *4*, 1900608.
- [31] A. Chandrasekhar, V. Vivekananthan, G. Khandelwal, W. J. Kim, S. J. Kim, *Mater. Today Energy* **2020**, *18*, 100544.
- [32] W. J. Kim, V. Vivekananthan, G. Khandelwal, A. Chandrasekhar, S. J. Kim, *ACS Appl. Electron. Mater.* **2020**, *2*, 3100.
- [33] K. Venugopal, P. Panchatcharam, A. Chandrasekhar, V. Shanmugasundaram, *ACS Sens.* **2021**, *6*, 1681.
- [34] A. Chandrasekhar, V. Vivekananthan, G. K Khandelwal, S. J. Kim, *ACS Sustainable. Chem. Eng.* **2020**, *8*, 4120.